Supporting Information

Zhang et al. 10.1073/pnas.1205266109

SI Experimental Procedures

Ventricular-Like Action Potential Simulation. The general method of modeling is similar to that used in the ten Tusscher model (1), in which the excitable cardiomyocyte is modeled as a capacitor connected with variable resistances and batteries representing the different ionic currents and pumps. In our modeling, the electrophysiological behavior of a single cardiomyocyte is described as the differential equation $dV/dt = (I_{ion})/C_m$, where C_m is the capacitance per unit cell surface, V is the membrane potential, and I_{ion} is the net ionic current across the membrane. I_{stim} in the original ten Tusscher model was omitted due to the autonomous firing capability of the differentiated cardiomyocytes.

In the ten Tusscher model, the modeling of action potentials (APs) for different types of cells (Epi, M, and Endo) in ventricular tissues was achieved by altering the maximum conductance of several ionic currents without altering their gating properties. The same method was adopted to simulate APs resembling those recorded from healthy control iPSC-derived cardiomyocytes. Basically, the maximum conductance of I_{CaL}, I_{K1}, and I_{Kr} was altered, whereas maximum conductance of other ionic components and all of the parameters regarding gating properties remained unchanged. To predict the disease phenotype of long QT syndrome type 3 (LQT3) and the pharmacological effect of late sodium channel blockers, an additional component I_{NaL} was incorporated into this model. The hyperpolarization-activated "funny current" I_f was also included to give rise to spontaneous firing capability in this system. The numerical reconstruction of I_{NaL} and I_f was based on Hodgkin and Huxley-type equations from the published literature (2) (see equations below):

$$I_{ion} = I_{Na} + I_{K1} + I_{to} + I_{Kr} + I_{Ks} + I_{CaL} + I_{NaCa} + I_{NaK} + I_{pCa} + I_{pK} + I_{bCa} + I_{bNa} + I_{NaL} + I_f \quad \textbf{[S1]}$$

$$\frac{dV}{dt} = -\frac{I_{ion}}{C_m} \quad \textbf{[S2]}$$

$$I_{Kr} = G_{Kr}\sqrt{\frac{K_0}{5.4}}x_{r1}x_{r2}(V - E_k) \quad \textbf{[S3]}$$

$$I_{Ks} = G_{Ks}x_s^2(V - E_{Ks}). \quad \textbf{[S4]}$$

Eq. **S1** shows all of the ionic components included in this simulation study. Eq. **S2** shows how net ionic current flux changes membrane potential. The Hodgkin–Huxley type Eq. **S3** shows the numeric construction of I_{Kr} current. G_{Kr}, maximum I_{Kr} conductance; K_o, extracellular potassium concentration; x_{r1}, open probability of activation gate; x_{r2}, open probability of inactivation gate; V, membrane potential; E_k, reversal potential of the potassium current. The Hodgkin–Huxley-type Eq. **S4** shows the numeric construction of I_{Ks} current. G_{Ks}, maximum I_{Ks} conductance; x_s, open probability of activation gate; E_{Ks}, reversal potential of the I_{Ks} current.

To predict the potential effect of I_{Kr} modulators on action potential, the inactivation $V_{1/2}$ of the x_{r2} gate and time constant of activation/deactivation of the x_{r1} gate were manipulated in a manner similar to that in the published literature (3). The detailed numerical reconstruction of I_{Kr} is also listed (see equations in *Numerical reconstitution of* I_{Kr} *current*). All simulations were written in C^{++} and run on a PC Intel Pentium Dual-Core, 2.60 GHz. The source code and other modeling information are available via www.hergcentral.org.

Numerical reconstitution of I_{NaL}.

$$E_{NaL} = \frac{RT}{F}\ln\left(\frac{[Na^+]_o}{[Na^+]_i}\right)$$

$$\alpha_{m,L} = \frac{0.32(V_m + 47.13)}{1 - \exp(-0.1(V_m + 47.13))}$$

$$\beta_{m,L} = 0.08\exp\left(\frac{-V_m}{11.0}\right)$$

$$h_{L,\infty} = \frac{1}{1 + \exp((V_m + 91)/6.1)}$$

$$\tau_{HL} = 600\text{ms}$$

$$I_{NaL} = G_{NaL}m_L^3h_L(V_m - E_{NaL}).$$

Numerical reconstitution of I_f.

If $V_m < -80$ mV,

$$y_\infty = 0.01329 + \frac{0.99921}{1 + \exp((V_m + 97.134)/8.1752)}.$$

If $V_m \geq -80$ mV,

$$y_\infty = 0.0002501\exp(-V_m/12.861)$$

$$\tau_y = \frac{1{,}000}{\frac{0.36(V_m + 148.8)}{\exp(0.066(V_m + 148.8)) - 1} + \frac{0.1(V_m + 87.3)}{1 - \exp(-0.21(V_m + 87.3))}} - 54$$

$$I_f = G_f y(V_m - E_f)E_f = -22\text{ mV}.$$

Numerical reconstitution of I_{Kr} current.

$$x_{r1\infty} = \frac{1}{1 + \exp((-26 - V_m)/7)}$$

$$\alpha_{xr1} = \frac{450}{1 + \exp((-45 - V_m)/10)}$$

$$\beta_{xr1} = \frac{6}{1 + \exp((V_m + 30)/11.5)}$$

$$\tau_{xr1} = \alpha_{xr1}\beta_{xr1}$$

$$x_{r2\infty} = \frac{1}{1 + \exp((V_m + 88)/24)}$$

$$\alpha_{xr2} = \frac{3}{1 + \exp((-60 - V_m)/20)}$$

$$\beta_{xr2} = \frac{1.12}{1 + \exp((V_m - 60)/20)}$$

$$\tau_{xr2} = \alpha_{xr2}\beta_{xr2}$$

$$I_{Kr} = G_{Kr}\sqrt{\frac{K_o}{5.4}}x_{r1}x_{r2}(V_m - E_K).$$

iPSC Culture and in Vitro Cardiac Differentiation. Human iPS cell lines from the patient with long QT1 syndrome and the healthy control (4) were maintained in feeder-free mTeSR1 medium (Stemcell Technologies) on matrigel-coated (BD Bioscience) plates at 37 °C with 5% (vol/vol) CO_2, according to protocols provided by WiCell Research Institute (Madison, WI).

The iPS cell lines were differentiated via embryoid body (EB) formation using a previously described protocol (4), with minor modifications. Briefly, on day 0 of differentiation, iPS cells were detached by accutase (Invitrogen) and seeded at 0.5×10^6/mL in mTeSR1 medium supplemented with 10 μM Rho-Associated Coil Kinase inhibitor, Y-27632 (EMD Biosciences), and 100 ng/mL Activin A (R&D Systems) in six-well ultra-low attachment plates (Corning). The medium was replaced with fresh mTeSR1 medium on day 1 for the cells from the patient with LQT1 or day 2 for the healthy control cells and replaced on day 4 with EB20 cardiac differentiation medium containing 50/50 DMEM/F-12 (Invitrogen) supplemented with 20% FBS (Thermo Fisher Scientific), 50 μg/mL ascorbic acid (Sigma-Aldrich), 3.5 mM L-glutamine (Invitrogen), 1% MEM nonessential amino acids (Invitrogen), and 0.1 mM 2-mercaptoethanol (Invitrogen). Embryoid bodies were maintained in suspension for 3 d and plated on 0.1% gelatin-coated (Sigma-Aldrich) plates on day 7. Areas exhibiting spontaneous contraction were observed usually from day 9 of differentiation onward. These beating clusters were microdissected and plated on gelatin-coated plates between days 15 and 20. They were maintained in culture in the EB2 media containing 50/50 DMEM/F-12 (Invitrogen) supplemented with 2% FBS (Thermo Fisher Scientific), 3.5 mM L-glutamine (Invitrogen), 1% MEM nonessential amino acids (Invitrogen), and 0.1 mM 2-mercaptoethanol (Invitrogen).

Dissociation of Beating Clusters for Electrophysiological Recording. For whole-cell patch-clamp recordings, 2- to 3-mo-old beating clusters were microdissected and disaggregated as previously reported (5, 6). Briefly, beating clusters were manually dissected and incubated in buffer 1 (120 mM NaCl, 5.4 mM KCl, 5 mM $MgSO_4$, 5 mM sodium pyruvate, 20 mM taurine, 10 mM Hepes, 20 mM glucose, pH 6.9) for 30 min at room temperature, in buffer 2 (120 mM NaCl, 5.4 mM KCl, 0.03 mM $CaCl_2$, 5 mM $MgSO_4$, 5 mM sodium pyruvate, 20 mM taurine, 10 mM Hepes, 20 mM glucose, 1 mg/mL collagenase A, pH 6.9) for 45 min at 37 °C with 5% CO_2, and in buffer 3 (85 mM KCl, 30 mM K_2HPO_4, 5 mM $MgSO_4$, 5 mM sodium pyruvate, 20 mM taurine, 1 mM EGTA, 5 mM creatine, 20 mM glucose, 2 mM Na_2ATP, pH 7.2) for 60 min at room temperature. Clusters were further dissociated by repetitively pipetting through a P1000 tip. Small clusters of 5–20 cells and single cells were plated on fibronectin-coated (Sigma-Aldrich) coverslips for electrophysiological analysis.

Chinese Hamster Ovary Cell Culture. Chinese hamster ovary (CHO) cells stably coexpressing KCNQ1 and KCNE1 were grown in 50/50 DMEM/F-12 (Mediatech) with 10% FBS (Gemini Bio-products) and 2 mM L-glutamine (Invitrogen). CHO cells stably expressing hERG were grown in F12, GlutaMAX (Invitrogen) with 10% FBS (Gemini Bio-products).

Quantitative Real-Time PCR. Total mRNA was isolated from control and LQT1 iPSC-derived cardiomyocyte clusters, using the Stratagene Absolutely RNA kit. RNA from cardiomyocyte explants and human adult and fetal heart (Clontech) was linearly amplified using the RNA Amplification RampUP Kit (Genisphere) and subsequently 1 μg of amplified RNA was used to synthesize cDNA with the High-Capacity cDNA Reverse Transcription kit (Applied Biosystems). Gene expression was quantified by quantitative real-time (qRT)-PCR, using 1 μL of the RT reaction and the Power SYBR Green PCR Master Mix (Applied Biosystems). The following primers were used: *HERG1a*, forward-GGCTCATGACACCAACCAC, reverse-TTCAGGCGGAAGGTCTTG; *HERG1b*, forward-ACGCTTACTGCCAGGGTGAC, reverse-GCCGACTGGCAACCAGAG; *KCNQ1*, forward-CGCCTGAACCGAGTAGAAGA, reverse-TGAAGCATGTCGGTGATGAG; *GAPDH*, forward-TCCTCTGACTTCAACAGCGA, reverse-GGGTCTTACTCCTTGGAGGC. Gene expression levels were normalized to *GAPDH*.

Electrophysiological Recording in CHO Cells and iPSC-Derived Cardiomyocytes. Traditional whole-cell voltage-clamp recording was performed at room temperature to record the hERG currents in CHO cells with an Axopatch-200A amplifier (Molecular Devices). The pipette solution contained 145 mM KCl, 1 mM $MgCl_2$, 5 mM EGTA, 10 mM Hepes, 5 mM Mg-ATP (pH 7.3 with KOH); the extracellular solution contained 140 mM NaCl, 5 mM KCl, 2 mM $CaCl_2$, 1 mM $MgCl_2$, 10 mM Hepes, 10 mM glucose (pH 7.4 with NaOH). Capacitance and 60–80% series resistance were routinely compensated.

To reduce the rundown of the KCNQ1/KCNE1 current, whole-cell recording was performed in a perforated-patch configuration at room temperature (6). The pipette solution contained 25 mM KCl, 120 mM K-aspartate, 1 mM $MgCl_2$, 1 mM $CaCl_2$, 10 mM EGTA, 5 mM Hepes (pH 7.2 with KOH). Amphotericin B (Sigma-Aldrich) at 500 μg/mL was included in the pipette solution. The extracellular solution has the same composition as the one used in the hERG current recording. Series resistance was routinely compensated by 60–80%.

To record the spontaneous action potentials (sAPs) from differentiated cardiac myocytes, the Giga-Ohm seal was achieved under the voltage-clamp mode and the sAPs were collected under the current-clamp configuration using an Axopatch-200A amplifier (Molecular Devices). Cardiomyocyte clusters of 5 ∼ 20 cells with spontaneous contractions were selected for recordings. A perforated patch was used to prolong recording stability. The pipette solution contained 25 mM KCl, 120 mM K-aspartate, 1 mM $MgCl_2$, 1 mM $CaCl_2$, 10 mM EGTA, 5 mM Hepes, 4 mM Na_2-ATP, 2 mM Na-GTP (pH 7.2 with KOH). Amphotericin B (Sigma-Aldrich) at 500 μg/mL was included in the pipette solution. The extracellular buffer is modified Tyrode's solution containing 140 mM NaCl, 5.4 mM KCl, 1.3 mM $CaCl_2$, 0.5 mM $MgCl_2$, 5 mM Hepes, 5.5 mM glucose (pH 7.4 with NaOH). Recordings were performed at 30 °C. Junction potentials were subtracted after recording. To examine compound effects on native I_{Kr} and I_{Ks} currents, traditional whole-cell voltage-clamp recording was used. The external NaCl (126 mM) was replaced by 126 mM choline chloride and the solution was supplemented with 0.2 mM $CdCl_2$, 0.5 mM $BaCl_2$, 5 mM 4-AP, to suppress I_{Na}, I_{Ca}, I_{K1}, and I_{to}, respectively. The external solution contained 10 mM Hepes and pH was adjusted to pH 7.4 by NaOH. To record Kv4.3 and Nav1.5, the same external solution for hERG recording was used. To record Kir2.1 current, the external NaCl (140 mM) was replaced by 140 mM KCl. To record Cav1.2 current, the external solution contained 110 mM NaCl and 20 mM $BaCl_2$.

Electrodes were pulled from borosilicate glass capillaries (World Precision Instruments). When filled with the intracellular solution, the electrodes have typical resistance of 2–5 MΩ. During the recording, constant perfusion of extracellular solution was main-

tained using a BPS perfusion system (ALA Scientific Instruments). Electrical signals were filtered at 2 kHz and acquired with pClamp 9.2 software via a DigiData-1322A interface (Molecular Devices).

Data Acquisition and Analysis. For recordings on differentiated ventricular-like cardiomyocytes, the maximum diastolic potential (MDP) of clusters varied from −70 mV to ∼ −50 mV, action potential amplitude (APA) was greater than 70 mV, and action potential duration $(APD)_{90}/APD_{50}$ was less than 1.25. Only those cardiomyocytes satisfying the above criteria were included in the analysis. The analysis was performed by a customized program written by Matlab (MathWorks). Key parameters for action potentials were quantified, including APA, APD_{50} (50% repolarization duration), APD_{90} (90% repolarization duration), dV/dt_{Max} (maximum rising rate of the action potential upstroke), MDP, and APD_{90}/APD_{50}. The steady-state values are defined as, for a given parameter α, $|\alpha_{n+1} - \alpha_n| < 1/2{,}000$. Only steady-state values are used for quantitative analysis.

Statistics. Statistical significance was determined by paired or unpaired Student's *t* test (two-tail) for two groups as indicated (Excel; Microsoft). $^{*}P < 0.05$ was considered statistically significant and $^{**}P < 0.01$.

Compound. The Molecular Library Small Molecule Repository is provided by Evotec OAI. Individual compounds used were either custom synthesized or acquired from commercial sources including Chembridge, ChemDiv, and Enamine.

1. Bankston JR, et al. (2007) A novel and lethal de novo LQT-3 mutation in a newborn with distinct molecular pharmacology and therapeutic response. *PLoS ONE* 2:e1258.
2. Schwartz PJ, et al. (1995) Long QT syndrome patients with mutations of the SCN5A and HERG genes have differential responses to Na+ channel blockade and to increases in heart rate. Implications for gene-specific therapy. *Circulation* 92:3381–3386.
3. Zhou J, et al. (2005) Novel potent human ether-a-go-go-related gene (hERG) potassium channel enhancers and their in vitro antiarrhythmic activity. *Mol Pharmacol* 68: 876–884.
4. Cardona K, et al. (2010) Effects of late sodium current enhancement during LQT-related arrhythmias. A simulation study. *Conf Proc IEEE Eng Med Biol Soc* 2010:3237–3240.
5. Weerapura M, Nattel S, Chartier D, Caballero R, Hébert TE (2002) A comparison of currents carried by HERG, with and without coexpression of MiRP1, and the native rapid delayed rectifier current. Is MiRP1 the missing link? *J Physiol* 540:15–27.
6. Benson AP, Al-Owais M, Holden AV (2011) Quantitative prediction of the arrhythmogenic effects of de novo hERG mutations in computational models of human ventricular tissues. *Eur Biophys J* 40:627–639.

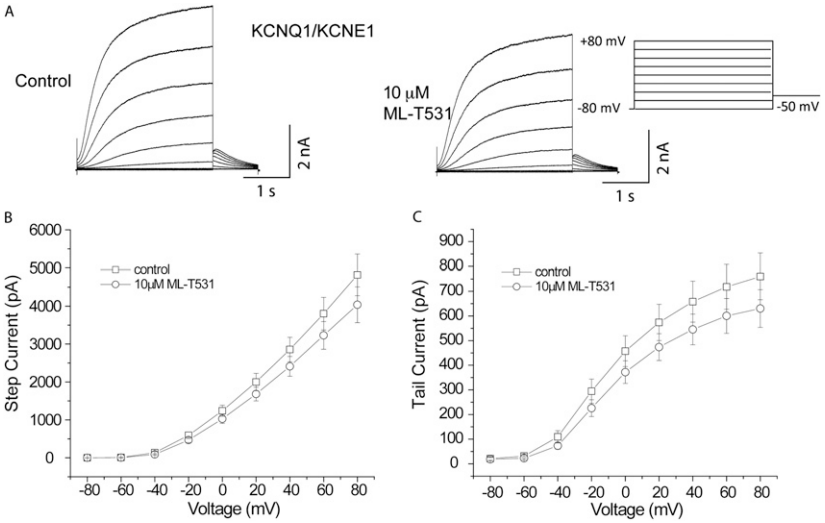

Fig. S1. ML-T531 effect on KCNQ1/KCNE1 current amplitude in a recombinant system. (*A*) ML-T531 does not potentiate KCNQ1/KCNE1 steady-state currents and tail currents in CHO cells. (*B*) ML-T531, at 10 μM modestly inhibits KCNQ1/KCNE1 currents elicited at depolarized step voltages. The holding potential was −80mV, and step current amplitude was tested at a given voltage for 3 s. (*C*) ML-T531 at 10 μM slightly inhibits KCNQ1/KCNE1 tail currents. The tail current amplitude was tested at −50 mV and plotted against the preceding step voltages indicated in the horizontal axis.

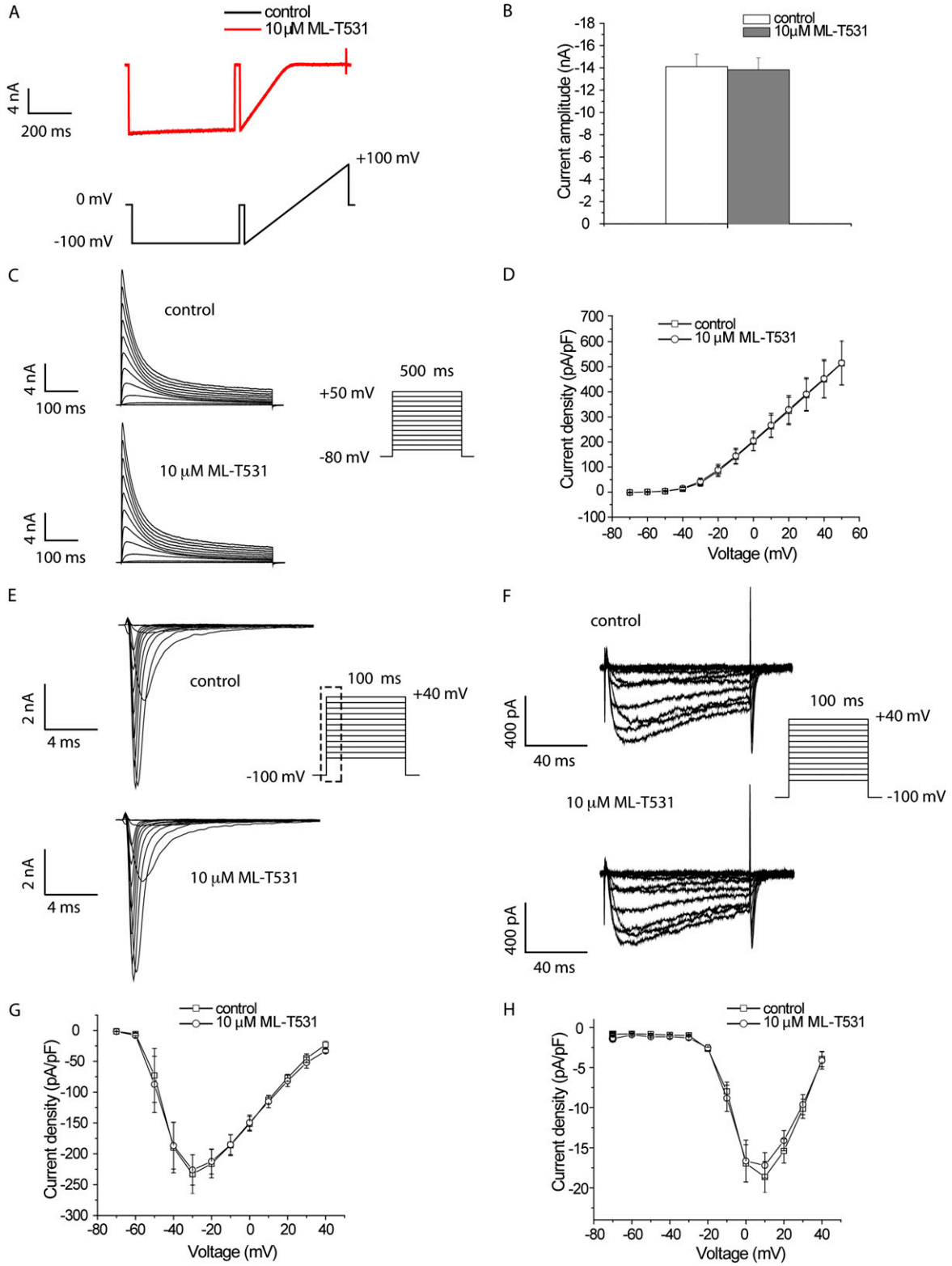

Fig. S2. Effects of ML-T531 on cloned cardiac ion channels. (*A*) Representative traces showing Kir2.1 currents in HEK cells in the presence and absence of T531 at 10 μM as indicated. (*B*) Histogram of Kir2.1 current elicited at −100 mV in the absence and presence of 10 μM ML-T531 (n = 6). (*C*) Representative traces showing Kv4.3 currents in HEK cells in the presence and absence of ML-T531 at 10 μM as indicated. The holding potential was −80 mV and Kv4.3 currents were elicited by 500-ms step depolarization ranging from −70 mV to +50 mV in 10-mV increments as shown (*Inset*). (*D*) Current–voltage plot showing effects of 10 μM ML-T531 on Kv4.3 currents over the range of indicated voltages (n = 6). (*E*) Representative traces showing Nav1.5 currents in HEK cells in the presence and absence of ML-T531 at 10 μM as indicated. The holding potential was −100 mV, and Nav1.5 currents were elicited by 100-ms step depolarizations ranging from −70 mV to +40 mV in 10-mV increments. For clarity, only currents recorded during the first 20 ms following depolarization are shown. (*F*) Representative traces showing Cav1.2 currents in HEK cells in the presence and absence of ML-T531 at 10 μM as indicated. The holding potential was −100 mV and Cav1.2 currents were elicited by 100-ms step depolarizations ranging from −70 mV to +40 mV in 10-mV increments. (*G*) Current–voltage plots showing average effects of ML-T531 on Nav1.5 peak currents (n = 6). (*H*) Current–voltage plots showing the average effects of ML-T531 on Cav1.2 currents (n = 6).

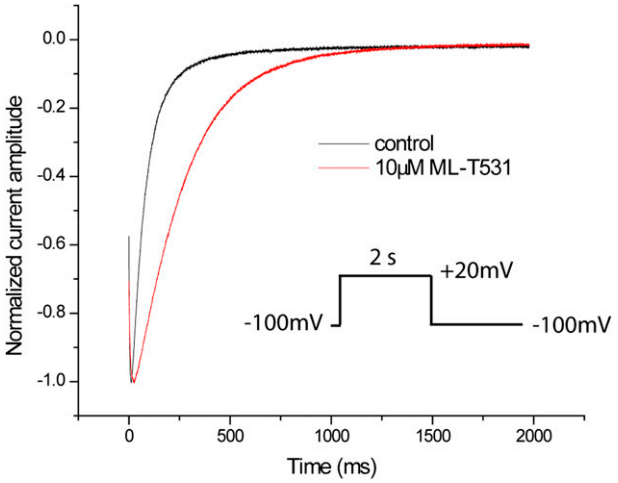

Fig. S3. ML-T531 effects on deactivation of hERG tail currents in a recombinant system ML-T531, at 10 μM, significantly slows the deactivation of hERG inward tail currents. Shown here are representative traces acquired from the same cell, in the absence or presence of ML-T531, after normalization to the peak current amplitude. The hERG channels were activated at +20 mV for 2 s and the inward tail currents were recorded at −100 mV.

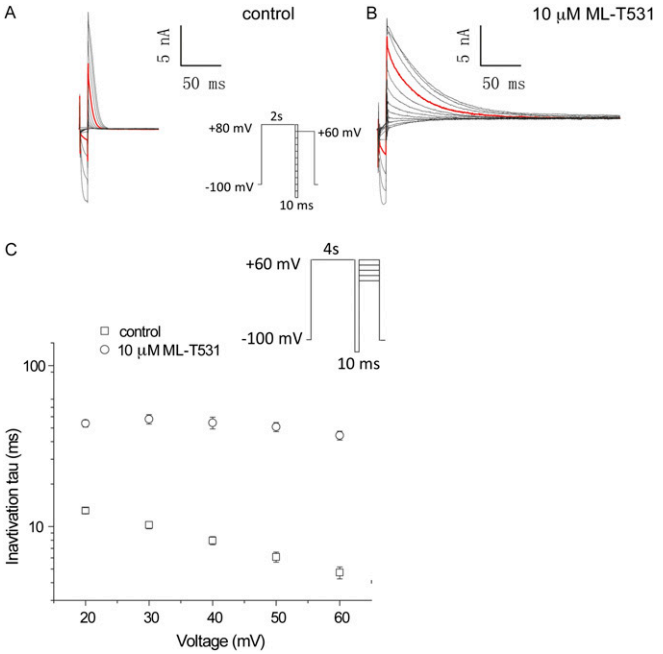

Fig. S4. ML-T531 effect on hERG current inactivation $V_{1/2}$ in a recombinant system. (*A* and *B*) Representative traces obtained from the same cell, with or without ML-T531 treatment as indicated. A three-step pulse protocol was used to determine hERG channel inactivation $V_{1/2}$. The hERG channels were fully activated at +80 mV for 2 s and channel inactivation was removed at different voltages for 10 ms. Then, the tail current was tested at +60 mV to examine the recovery of hERG channel from inactivation. The highlighted red line indicates the trace elicited at −80 mV. (*C*) Effect of ML-T531 on inactivation. Using the indicated protocol, the inactivation time constant was estimated and plotted according to the voltages.

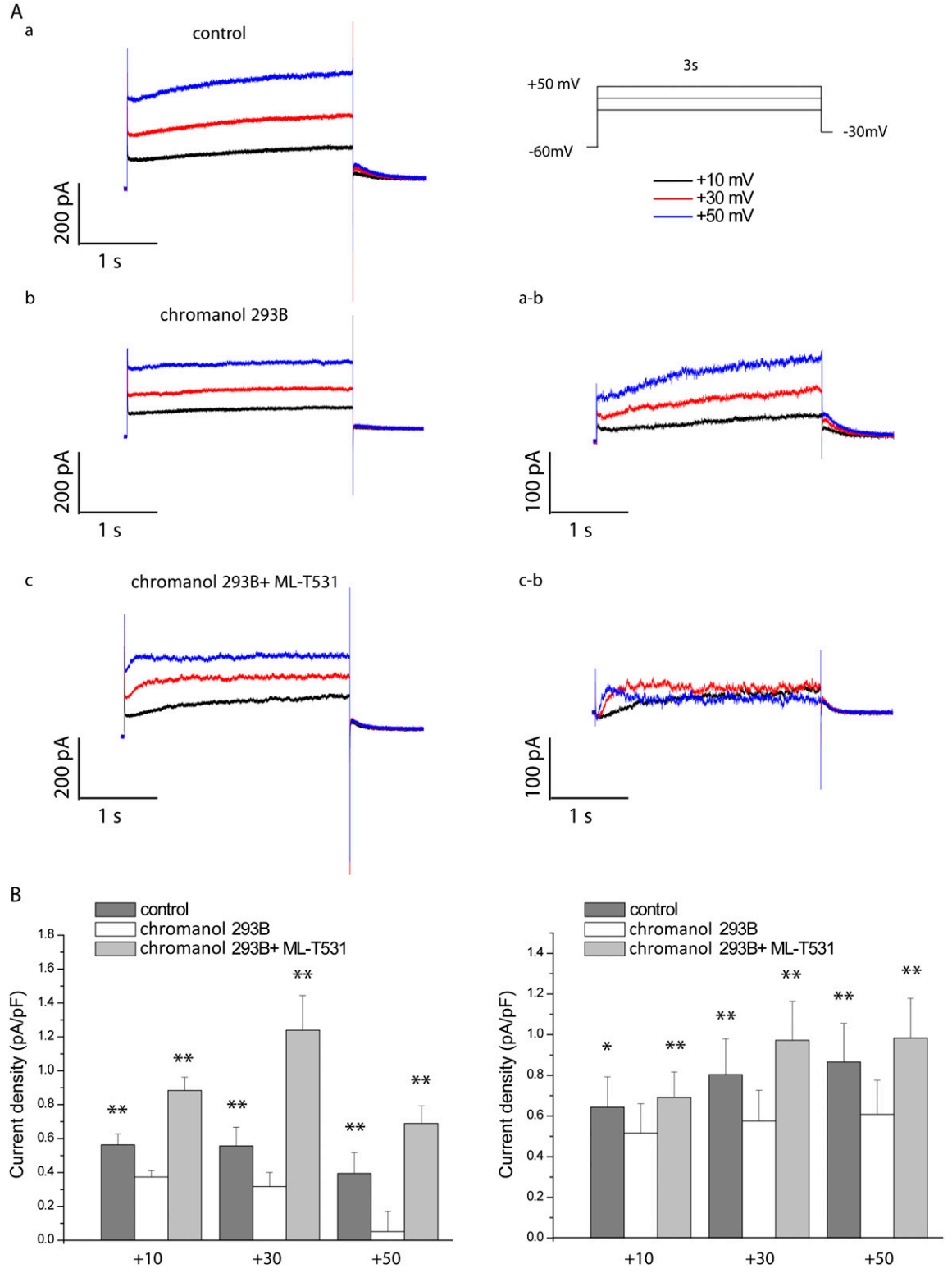

Fig. S5. ML-T531 potentiates native potassium currents in iPSC-derived cardiomyocytes in the presence of I_{Ks} inhibitor. (*A*) Representative traces recorded from an isolated differentiated cardiomyocyte. The holding potential was −60 mV. The steady-state currents were activated by depolarizing voltage steps from −10 mV to +50 mV in 20-mV increments as shown (*Inset*). The tail currents were measured at −30 mV. Excluding I_{Kr} and I_{Ks}, other major ionic components including I_{Na}, I_{K1}, I_{to}, and I_{CaL} were pharmacologically suppressed under the recording conditions (*SI Experimental Procedures*). Currents from a representative cell are shown following different compound treatments as indicated. (*B*) Summary of compound effects on steady-state current (*Left*) and tail current (*Right*) amplitudes at the indicated voltages ($n = 6$). The statistical analysis was performed pairwise between the control group and the chromanol 293B-treated group and between the chromanol 293B-treated group and the chromanol 293B plus ML-T531–treated group. (*$P < 0.05$; **$P < 0.001$).

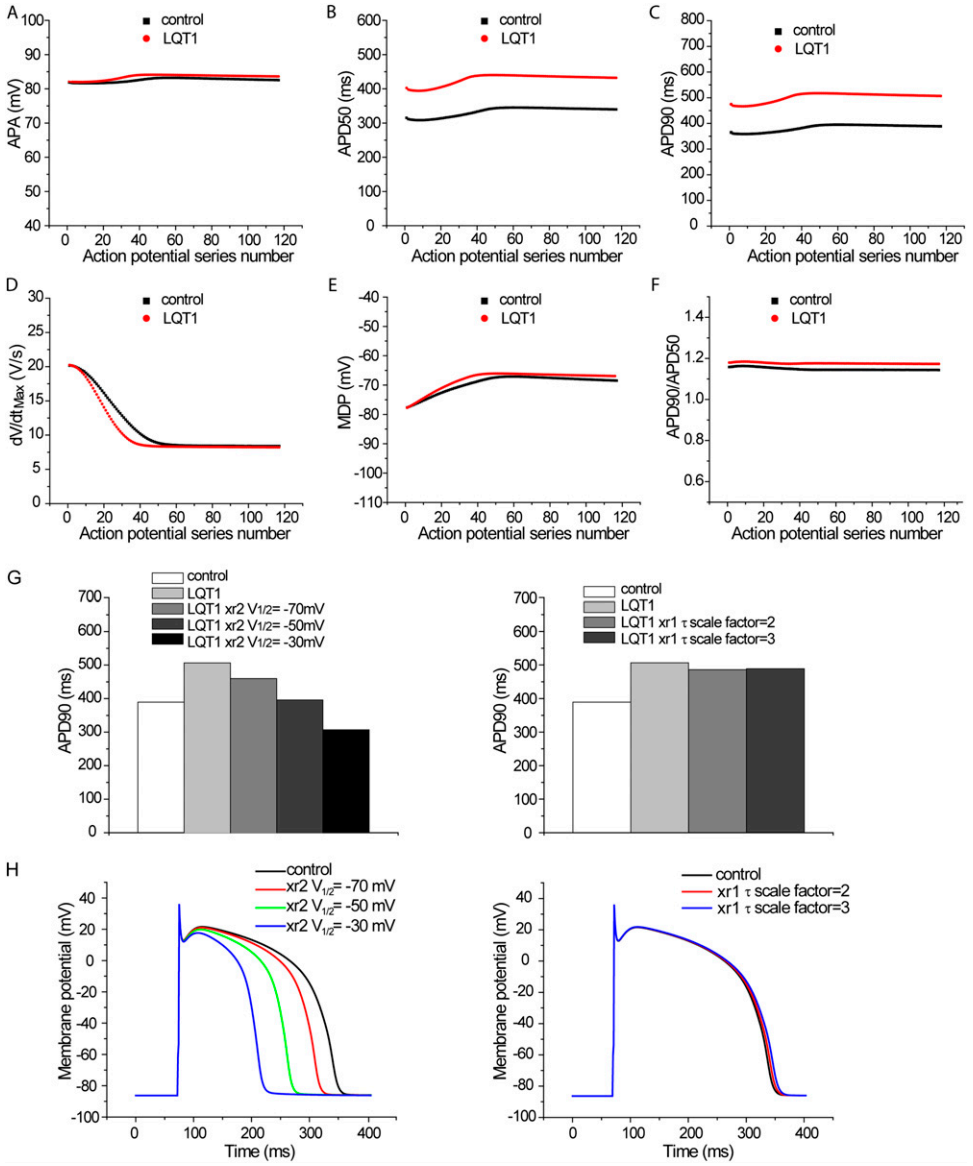

Fig. S6. Modeling of cardiac myocyte electrical properties using the modified ten Tusscher model and the original ten Tusscher model. (*A–F*) Using the modified ten Tusscher model, several important parameters (APA, APD_{50}, APD_{90}, dV/dt_{Max}, MDP, and APD_{90}/APD_{50}) are plotted for the first 120 spontaneously generated action potentials using either control myocyte parameters or parameters specific for LQT1 myocytes. (*G*) Predicted effects of I_{Kr} gating modifiers on steady-state action potentials using the modified ten Tusscher model. (*Left*) Depolarizing shifts in I_{Kr} inactivation $V_{1/2}$ decrease predicted APD_{90} values for LQT1 myocytes. (*Right*) Increasing I_{Kr} deactivation τ has minimal effects on predicted APD_{90} values for LQT1 myocytes. (*H*) Predicted effects of I_{Kr} gating modifiers on action potentials using the original ten Tusscher model. (*Left*) Depolarizing shifts in I_{Kr} inactivation $V_{1/2}$ increase action potential duration. (*Right*) Increasing I_{Kr} deactivation τ produces minimal effects on action potential duration.

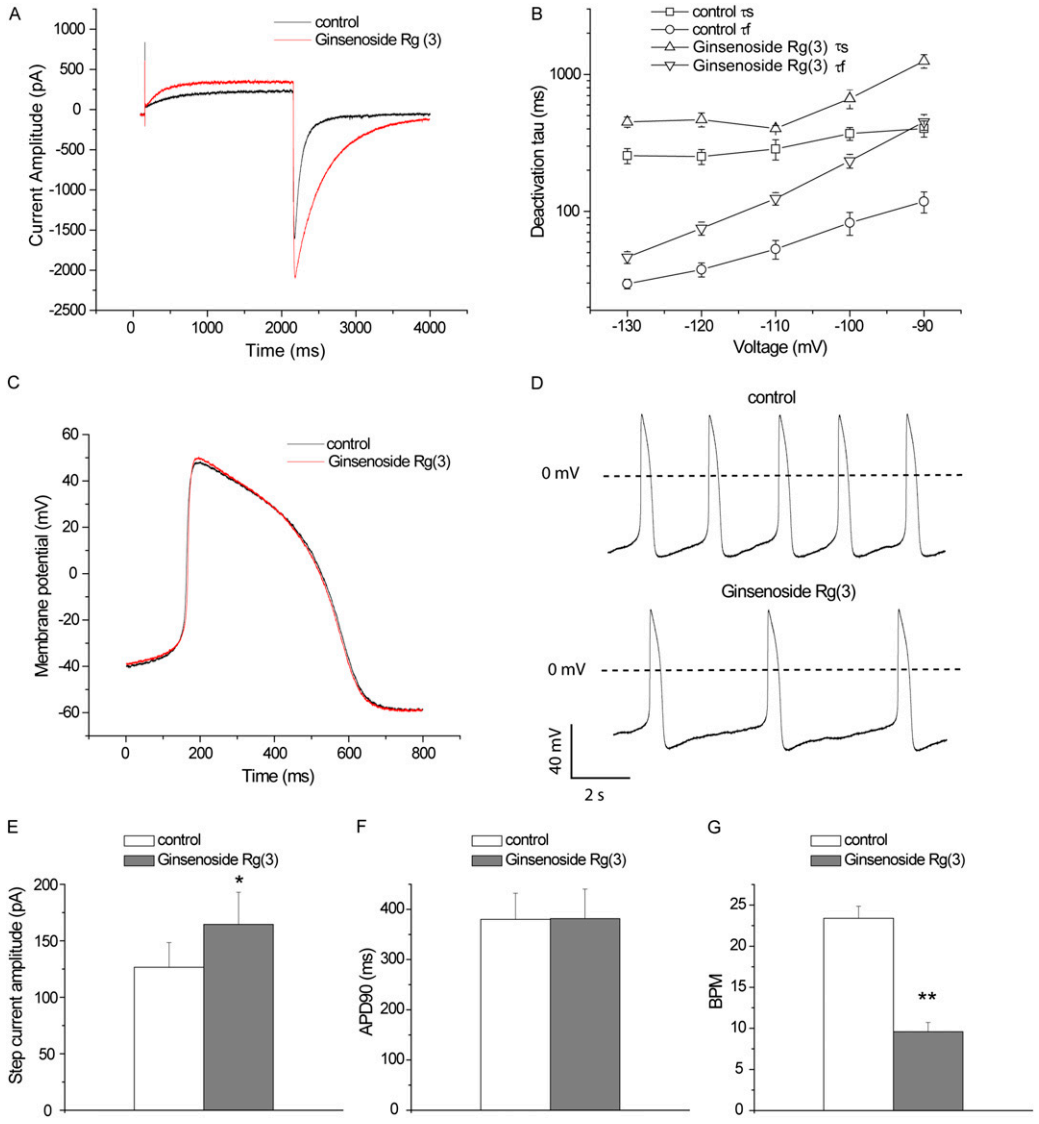

Fig. S7. Ginsenoside Rg(3) effects on hERG currents and action potentials recorded from human iPSC-derived cardiomyocytes. (*A*) Representative traces showing 1 μM Ginsenoside Rg(3) effects on hERG currents expressed in CHO cells. The holding potential was −100 mV. The steady-state current was tested at +20 mV, and the tail current was elicited at −100 mV. (*B*) Deactivation kinetics of hERG in the presence and absence of 1 μM Ginsenoside Rg(3) were examined at indicated voltages after 2-s step depolarization at +20 mV. Tail current deactivation was fitted by a standard double-exponential equation and time constants are plotted in the absence and presence of 1 μM Ginsenoside Rg(3) ($n = 7$). (*C*) Representative traces showing 1 μM Ginsenoside Rg(3) effects on single action potentials of human iPSC-derived cardiomyocytes. (*D*) Representative traces showing 1 μM Ginsenoside Rg(3) effects on the spontaneous action potential frequency of cardiomyoctes. (*E*) Histogram showing 1 μM Ginsenoside Rg(3) effects on the steady-state hERG current amplitudes recorded at +20 mV from CHO cells. (*F*) APD_{90} values of human iPSC-derived cardiomyocytes were examined in the presence and absence of 1 μM Ginsenoside Rg(3) ($n = 5$). (*G*) Histogram showing 1 μM Ginsenoside Rg(3) effects on spontaneous action potential frequency of the cardiomyocytes ($n = 5$). (*$P < 0.05$; **$P < 0.001$).

Table S1. Summary of values in ten Tusscher (TNNP) model and modified maximum conductance used in the current simulation

	TNNP model	Value used
G_{Na}	14.838 nS/pF	14.838 nS/pF
G_{K1}	5.405 nS/pF	0.03 × 5.405 nS/pF*
G_{to}	0.294 nS/pF	0.294 nS/pF
G_{Kr}	0.096 nS/pF	0.55 × 0.096 nS/pF*
G_{Ks}	0.245 nS/pF	0.245 nS/pF
G_{CaL}	1.75^{-4} $cm^3 \cdot \mu F^{-1} \cdot S^{-1}$	2×1.75^{-4} $cm^3 \cdot \mu F^{-1} \cdot S^{-1}$*
k_{NaCa}	1,000 pA/pF	1,000 pA/pF
P_{NaK}	1.362 pA/pF	1.362 pA/pF
G_{pCa}	0.025 nS/pF	0.025 nS/pF
G_{pK}	0.0146 nS/pF	0.0146 nS/pF
G_{bCa}	0.000592 nS/pF	0.000592 nS/pF
G_{bNa}	0.00029 nS/PF	0.00029 nS/PF
G_{NaL}	NA	0.055 nS/pF†
G_f	NA	0.009 nS/pF†

NA, not analyzed.

*Multiplicity factor over the value used in the ten Tusscher model.

†Values included in the current model that are absent in the ten Tusscher model.